Supplementary Information

In-situ Preparation of PHI/SnS_2 Heterojunction Photoanode towards Photoelectrochemical Applications

Zeyao He,[1] Xiaowei Lv, [1, 2*] Panpan Sun, [1] Doudou Zhang, [1*] Xiaohua Sun[1, 2*]

[1] *College of Materials and Chemical Engineering, Key Laboratory of Inorganic Nonmetallic Crystalline and Energy Conversion Materials, China Three Gorges University, Yichang, 443002, China*

[2] *Hubei Three Gorges Laboratory, Yichang, Hubei, 443007, China*

E-mail: xwlv@ctgu.edu.cn, mksxh@163.com

Materials

Dicyandiamide (AR), potassium thiocyanate (AR), anhydrous sodium sulfite, anhydrous ethanol, and acetone were purchased from Sinopharm Chemical Reagent Co., Ltd. Anhydrous stannous chloride (AR) was obtained from Aladdin Reagents Co., Ltd. Stannous sulfate (AR), potassium hydroxide (AR), sodium citrate (AR), and melamine (AR) were supplied by Shanghai Macklin Biochemical Co., Ltd. Deionized water was provided by a water purification system.

Photoelectrochemical Measurements

Photoelectrochemical measurements were performed using a CHI 760E electrochemical workstation (Shanghai Chenhua Instrument Co., Ltd., China) in a three-electrode configuration, where the reference electrode was Hg/HgO, the working electrode was the sample electrode, and the counter electrode was a Pt electrode. The electrolyte solution was 1 M KOH, and the light source was an AM 1.5G xenon lamp with an intensity of 100 mW cm^{-2}. The active area of the working electrode was processed to 1 × 1 cm^2, and the backside of the FTO substrate received the illumination.

Under irradiation, with a light-on time of 5 s and a light-off time of 5 s, linear sweep voltammetry (LSV) was used to measure the photocurrent density of the samples. Under the same conditions, but with a bias voltage of 0.31 V vs. Hg/HgO, the stability of the samples was evaluated using the I-t mode. Electrochemical impedance spectroscopy (EIS) was measured under irradiation with an AC signal amplitude of 10 mV. Mott-Schottky plots were recorded with an AC signal amplitude of 5 mV and a frequency of 1000 Hz.

The incident photon-to-current conversion efficiency (IPCE) was calculated using the formula: $IPCE = (1240 \times I_{SC}) / (\lambda \times P_{in})$, where ISC is the photocurrent density, Pin is the incident light power density, and λ is the wavelength of the incident light.

The potentials versus Hg/HgO were converted to those versus RHE according to the Nernst equation ($E_{RHE} = E_{Hg/HgO} + 0.059 \times pH + 0.098$). In addition, the conversion between E_{RHE} and E_{SHE} is carried out according to the following formula: $E_{RHE} = E_{SHE} + 0.059 \times pH$.

Characterization

The crystal structures of CN, PHI/SnS_2, and SnS_2 were characterized using an X-ray diffractometer (Rigaku SmartLab). The surface morphology of the photoanodes was examined using a field-emission scanning electron microscope (FE-SEM, JSM-7500F), and the elemental composition was determined by energy-dispersive X-ray spectroscopy (EDS) mapping. Fourier transform infrared (FTIR) spectroscopy was performed using a PerkinElmer Frontier Transform instrument. UV-visible absorption spectra were recorded using a Shimadzu UV-3600 iPlus spectrophotometer. Photoluminescence (PL) spectra were obtained using a Hitachi F4600 fluorescence spectrophotometer. Time-resolved photoluminescence spectra were measured using an Edinburgh Instruments FS5 spectrometer. X-ray photoelectron spectroscopy (XPS) was conducted on a Shimadzu AXIS Supra. The xenon lamp used was a Trusttech CHF-XM-500W, and the illumination was AM 1.5G. Spin coating was performed using a desktop spin coater (KW-4A, Institute of Microelectronics, Chinese Academy

of Sciences).

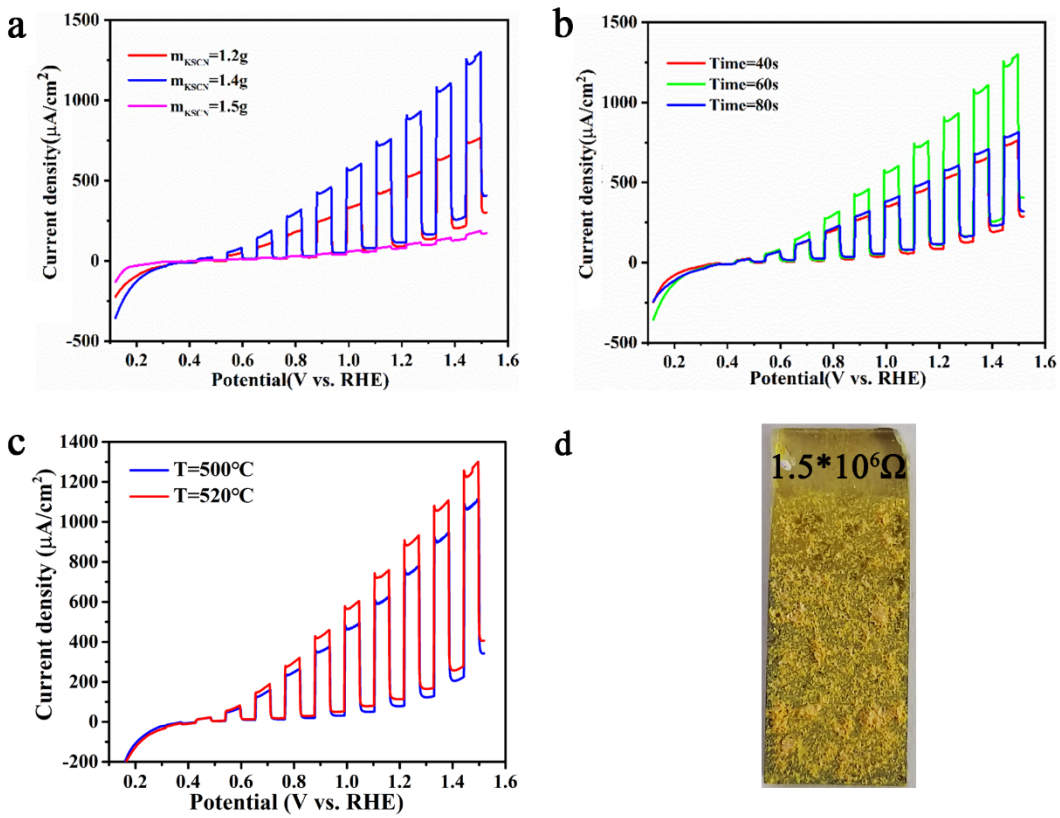

Figure S1. Light-on/off LSV curves of the PHI/SnS_2 photoanode in 1.0 M KOH solution under AM 1.5G illumination: (a) different amounts of KSCN, (b) different deposition time and (c) different deposition temperatures, (d) The optical image of PHI/SnS_2 photoanode prepared at 550°C.

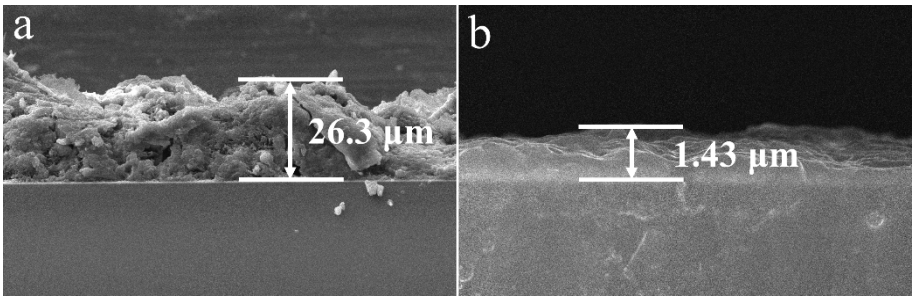

Figure S2. The thickness of PCN (a), PHI/SnS_2 (b)

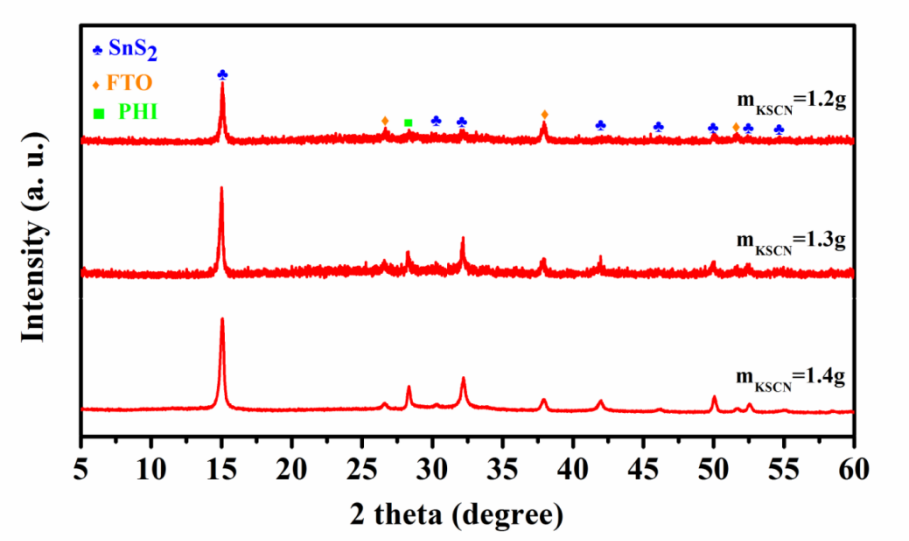

Figure S3. XRD pattern of the PCN/SnS_2 samples prepared by different KSCN content

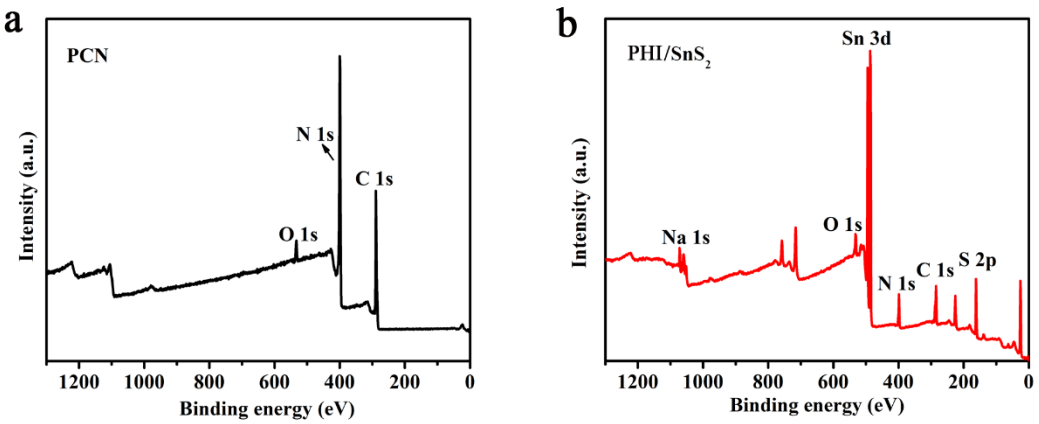

Figure S4. XPS full spectra of (a) PCN and (b) PHI/SnS_2 samples.

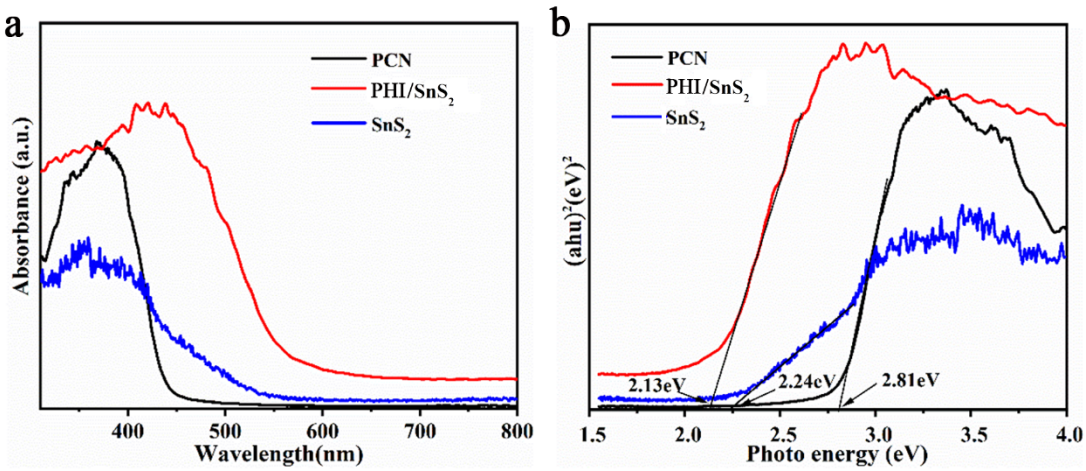

Figure S5. (a) UV-Vis spectra and (b) Tauc plots of PCN, PHI/SnS_2, and SnS_2 samples.

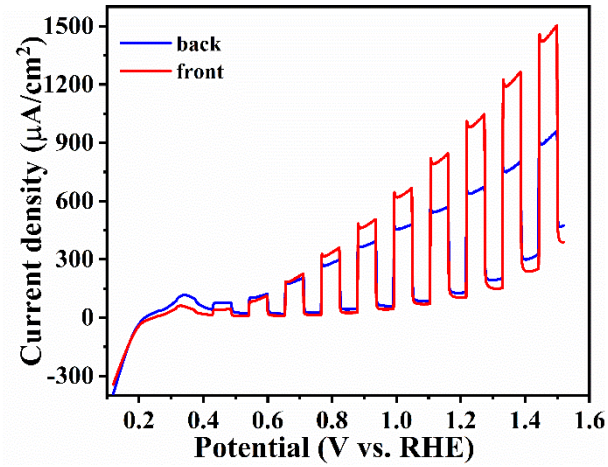

Figure S6. Light-on/off LSV curves of the PHI/SnS_2 photoanode in 1.0 M KOH solution under front or back illumination

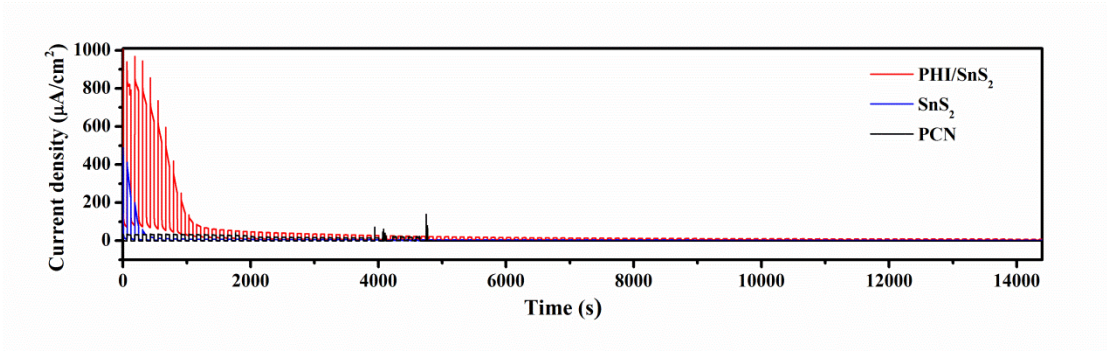

Figure S7. i-t curves of PCN, PHI/SnS_2, and SnS_2 photoanodes in 1.0 M KOH solution under AM 1.5G illumination.

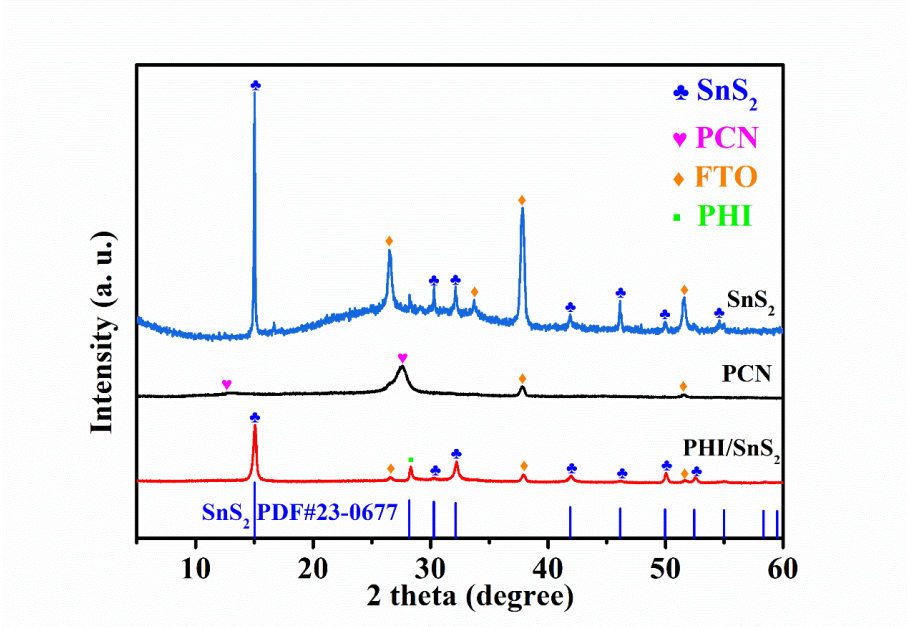

Figure S8. XRD patterns of PCN, PHI/SnS_2, and SnS_2 samples.

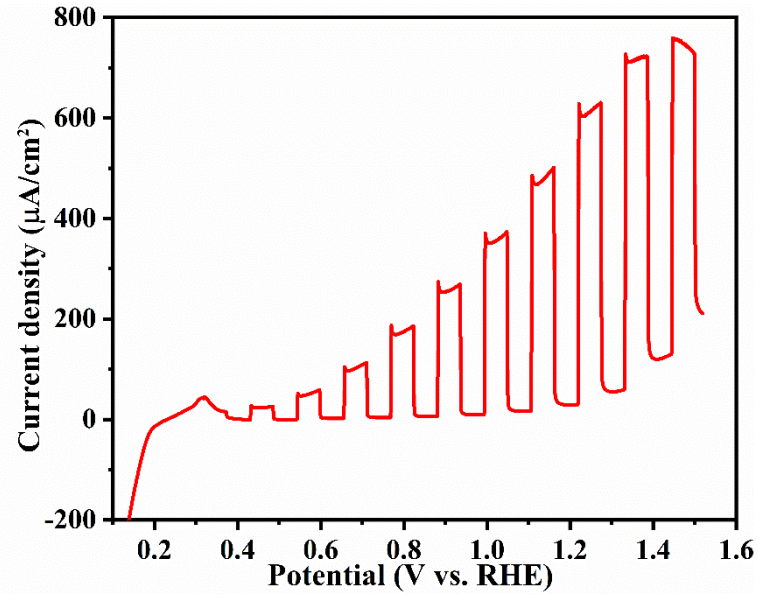

Figure S9. LSV curves of the SnS_2 photoanode in 1.0 M KOH solution under AM 1.5G illumination.

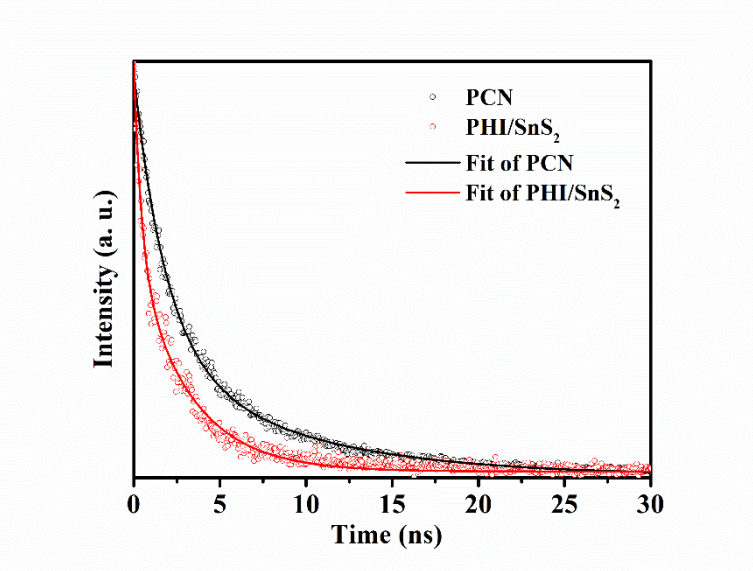

Figure S10.Time-resolved photo-luminescence decay spectra of PCN and PHI/SnS_2.

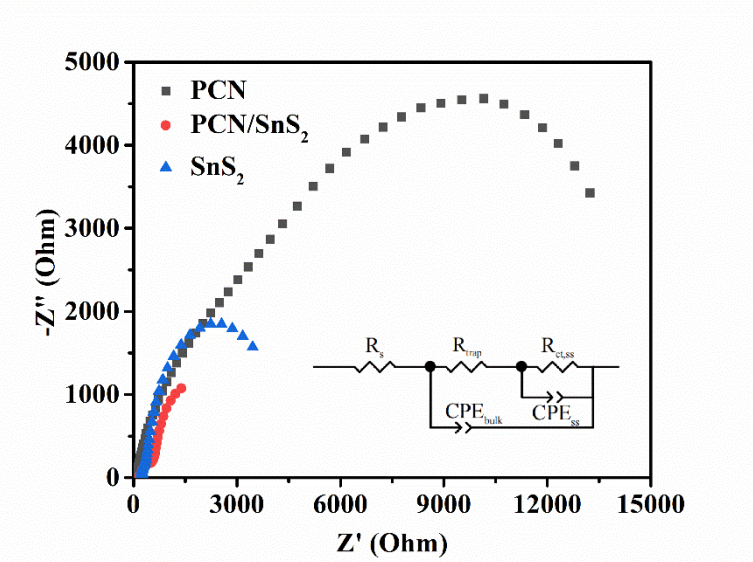

Figure S11. Nyquist plots of PCN, PHI/SnS_2, and SnS_2 photoanodes in 1.0 M KOH solution under AM 1.5G illumination, the inset showing the equivalent circuit diagram.

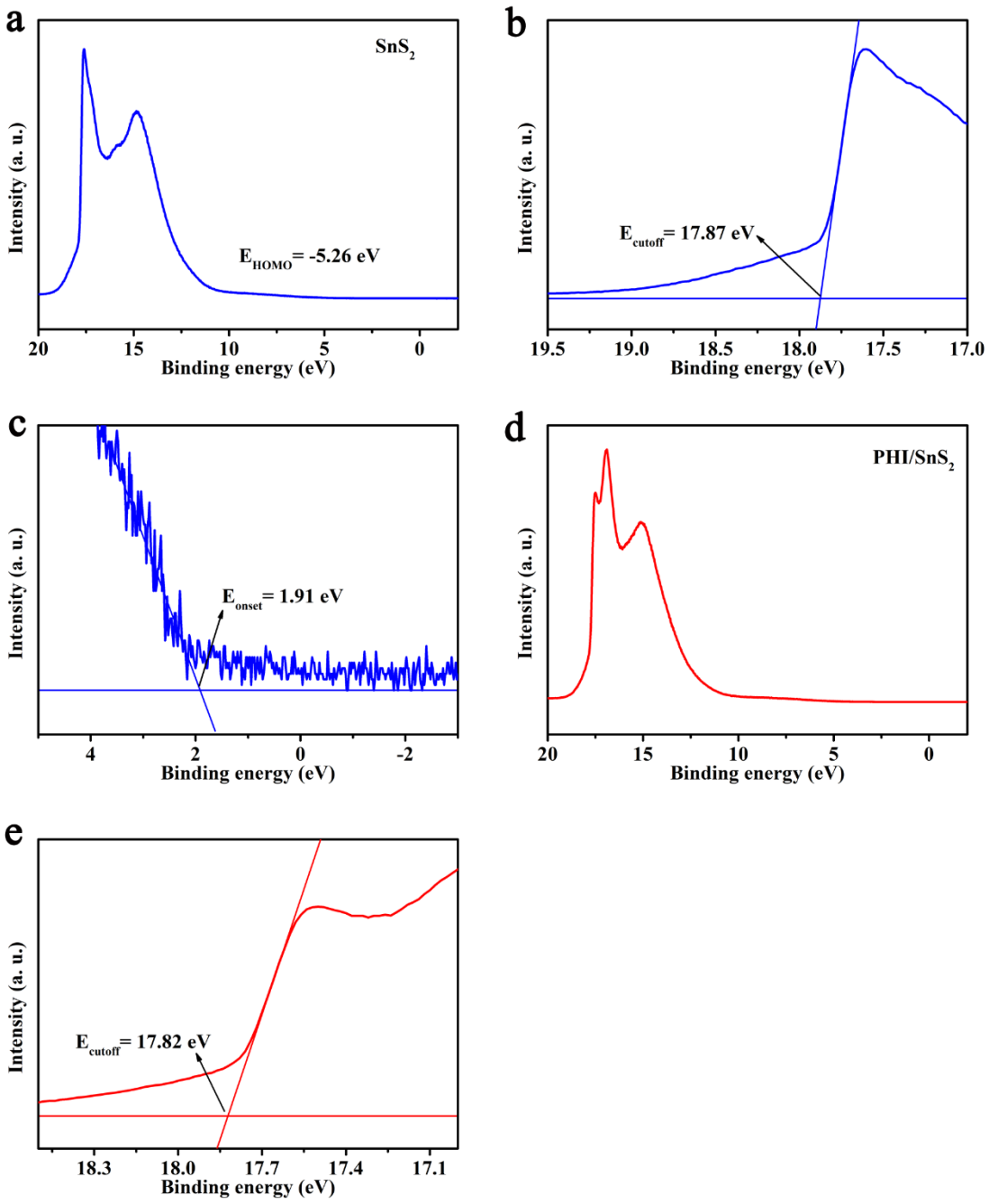

Figure S12. UPS spectra (a), the secondary edge region (b) and the HOMO region (c) of the SnS_2 sample, UPS spectra (d) and the secondary edge region (e) of the PHI/SnS_2 sample.

Table S1. Summary of PEC performance of this work and the reported PCN-based photoanodes.

Catalyst	Preparation method	Photocurrent Density ($\mu A\ cm^{-2}$)	Potential vs. RHE (V)	Electrolyte	Light source	Corresponding Author (Ref.)
PHI/SnS_2 photoanode	electrochemical deposition-chemical vapor deposition method	880	1.23	1.0 M KOH	100 mW cm^{-2}, AM 1.5G (Newport)	This work
K-PHI photoanode	Molten mediate polymerization	800	1.23	1.0 M NaOH	100 mW cm^{-2}, AM 1.5G (Newport)	[1]
CN-MR/$NiFeO_xH_y$ electrode	Doctor-blade echniqueassisted with CVD-like and solvothermal process	472 ± 10	1.23	0.1 M KOH	100 mW cm^{-2}, AM 1.5G (Newport)	[2]
CNTM photoanode	Seeded crystallization of CN monomers assisted with CVD-like process	353	1.23	0.1 M KOH	100 mW cm^{-2}, AM1.5G (Newport)	[3]
CN-$MSG_{0.75}$/M photoanode	Doctor-blade technique assisted with CVD-like process	270	1.23	0.1 M KOH	100 mW cm^{-2} , AM 1.5G (Newport)	[4]
CNP films	Evaporation polymerization	230	1.23	0.5 M Na_2SO_4	Xe lamp, AM 1.5G	[5]
CN films	Thermal vapor condensation	228.2	1.23	0.2 M Na_2SO_4	150 W Xe lamp, AM 1.5G (Newport)	[6]
P/B-layer-doping C_3N_4 photoanode	Thermal vapour deposition	150 ± 10	1.23	0.1 M Na_2SO_4	300 W Xe lamp, AM 1.5G	[7]
CN-MeM/$M_{0.20}$	Doctor-blade technique assisted with CVD-like process	133	1.23	0.1 M KOH	100 mW cm^{-2}, AM 1.5G (Newport)	[8]
SOCN-75 films	Thermal vapor condensation	119.2	1.23	0.1 M Na_2SO_4	150 W Xe lamp, AM 1.5G (Newport)	[9]
CN-CMK-s-MeOH photoanode	Solvothermal and doctor-blading	≈150	1.23	0.1 M KOH	100 W Xe lamp, AM 1.5G filter	[10]
KPCN photoanodes	alkali-assisted molten salts polymerization	162	1.23	1.0 M NaOH	300 W Xe lamp, AM 1.5G filter	[11]
CN-B/P films	close-spaced thermal copolymerization and drip coating-heat treatment technology	17.2 and 39.4	1.23	1.0 M KOH	100 mW cm^{-2}, AM 1.5G (Newport)	[12]
CN- Fe films	closed space copolymerization	32	1.23	1.0 M KOH	100 mW cm^{-2}, AM 1.5G (Newport)	[13]

Table S2. The fitted data of the impedance spectra

	Rs(Ω)	**R_{trap}(Ω)**	**$R_{ct,ss}$(Ω)**	**CPE_{bulk}-T(F)**	**CPE_{bulk}-P(F)**	**CPE_{ss}-T(F)**	**CPEss-P(F)**
PCN	83.8	5404	11576	1.0791×10^{-5}	0.7313	4.0489×10^{-5}	0.66818
PHI/SnS_2	185.3	552.2	2427	1.6961×10^{-4}	0.72897	7.5265×10^{-4}	0.97868
SnS_2	166.9	1089	7356	2.2303×10^{-4}	0.71281	1.2439×10^{-9}	4.87

Reference

1. X. Li, X. Chen, Y. Fang, W. Lin, Y. Hou, M. Anpo, X. Fu and X. Wang, *Chemical Science*, 2022, **13**, 7541-7551.
2. N. Karjule, C. Singh, J. Barrio, J. Tzadikov, I. Liberman, M. Volokh, E. Palomares, I. Hod and M. J. A. F. M. Shalom, *Adv. Funct. Mater*, 2021, **31**, 2101724.
3. J. Qin, J. Barrio, G. Peng, J. Tzadikov, L. Abisdris, M. Volokh and M. J. N. C. Shalom, *Nature Communications*, 2020, **11**, 4701.
4. N. Karjule, J. Barrio, L. Xing, M. Volokh and M. J. N. l. Shalom, *Nano letters*, 2020, **20**, 4618-4624.
5. Q. Jia, S. Zhang, Z. Gao, P. Yang, Q. J. C. S. Gu and Technology, *Catalysis Science & Technology*, 2019, **9**, 425-435.
6. W. Xiong, S. Chen, M. Huang, Z. Wang, Z. Lu and R. Q. J. C. Zhang, *ChemSusChem*, 2018, **11**, 2497-2501.
7. P. Luan, Q. Meng, J. Wu, Q. Li, X. Zhang, Y. Zhang, L. A. O'Dell, S. R. Raga, J. Pringle and J. C. J. C. Griffith, *ChemSusChem*, 2020, **13**, 328-333.

8. J. Xia, N. Karjule, L. Abisdris, M. Volokh and M. J. C. o. M. Shalom, *Chemistry of Materials*, 2020, **32**, 5845-5853.

9. M. Huang, H. Wang, W. Li, Y.-L. Zhao and R.-Q. J. J. o. M. C. A. Zhang, *Journal of Materials Chemistry A*, 2020, **8**, 24005-24012.

10. D. Garg, T. Shmila, G. Mark, S. Mondal, V. R. Battula, M. Volokh and M. Shalom, *Advanced Sustainable Systems*, 2023, **8**, 2300447.

11. X. Li, D. Zheng, W. Wu, X. Long, B. Yang, X. Huang, J. Duan, S. Liu, B. Lan and R. Cao, *New Journal of Chemistry*, 2024, **48**, 19452-19461.

12. L. Wang, D. Chen, S. Zhang, D. Zhang, X. Lv, P. Sun, N. Huang, L. Fang and X. Sun, *ChemistrySelect*, 2023, **8**, e202203688.

13. X. Yang, X. Lv, K. Tong, M. Peng, Z. He, P. Sun and X. Sun, *ChemPlusChem*, 2024, **89**, e202300650.